Low Voltage Ride-Through of a Grid-Connected Doubly-Fed Induction Generator with Speed Sensorless Vector Control

Saroja Kanti Sahoo, *Student Member, IEEE,* A. K. Sinha, *Member, IEEE*, N. K. Kishore, *Senior Member, IEEE*
Department of Electrical Engineering, Indian Institute of Technology Kharagpur, West Bengal, India
{sarojaksahoo, aksinha, kishor}@ee.iitkgp.ernet.in

***Abstract*— Doubly-fed induction generators (DFIG) are commonly employed in medium and high power applications for variable speed drives. Grid-connected DFIG based wind turbines are subject to sudden voltage dips caused by symmetrical and asymmetrical grid faults. According to new grid codes, DFIG based wind turbines should ride-through voltage dips without interrupting their operation. Hence, they should be capable of low voltage ride-through (LVRT) to maintain stable and safe operation of power system. Furthermore, for a practical DFIG, mounting a shaft speed sensor involves high cost, maintenance, and cabling issues. In this paper, a solution to both voltage dip and absence of a speed encoder is addressed for a 22 kW DFIG setup. A detailed mathematical modeling with sensorless vector control and protection against sudden voltage drop is studied and simulated in MATLAB/SIMULINK environment.**

Keywords—Doubly fed induction machine, MRAS, sensorless, Low voltage ride- through (LVRT)

I. Introduction

Doubly fed induction generators (DFIG) based wind turbines are popular due to their applications in variable speed drives, decoupled control of active and reactive power, and reduced converter power rating [1]. It is commonly used with back-to-back converter arrangement with stator being directly connected to grid and rotor power being fed through rotor side converter (RSC) [2]. For a DFIG based wind generator setup, mounting a shaft speed sensor is problematic due to its cost, maintenance, and cabling issues [3, 4]. Model reference adaptive system (MRAS) based sensorless vector control techniques have several advantages over other speed estimation methods as they are robust and remain unaffected by plant's parameter variation and load disturbance effect [5]. Some of the widely employed MRAS techniques for sensorless vector control are stator-flux, rotor-flux, stator current, and rotor current MRAS techniques [3, 4]. The review in [3] suggested that rotor current-based MRAS technique is immune to integrator drift at the low excitation frequency and is independent of resistance parameters.

Grid-connected DFIG could be subject to regular grid disturbances such as symmetrical and asymmetrical faults giving rise to voltage dips at the point of common coupling of wind turbines. Due to the sudden voltage dip, the stator current magnitude increases significantly. As a result, large transients are observed in rotor current, and there is a dc link overvoltage too. In [6], a solution to voltage dip problem was addressed by including an anti-parallel thyristor-based bypass arrangement in the rotor circuit and providing reactive power to the grid during the disturbance. A survey of existing LVRT techniques for DFIG-based wind turbines is explored in [8]. In [10], a crowbar system in the rotor circuit and a dc chopper aids the LVRT operation with sliding mode controllers operating the converters.

Speed sensorless vector control and LVRT of DFIG are two independent and broadly researched topics. However, rarely it is found that both sensorless and LVRT capability being addressed for DFIG-based wind energy conversion system. In this paper, rotor current-based MRAS sensorless vector control with protection provided by crowbar arrangement, GTO-based thyristor controlled stator current limiter and dc chopper is used for the grid-connected DFIG-based wind turbine. The entire system as shown in Fig. 1 is modeled in MATLAB/SIMULINK environment. Sections II, III, IV and V discuss the modeling of DFIG, sensorless vector control of rotor side converter, supply side converter control, and LVRT technique of DFIG respectively. Sections VI and VII present the results and discussion part. Finally, Section VIII concludes the paper.

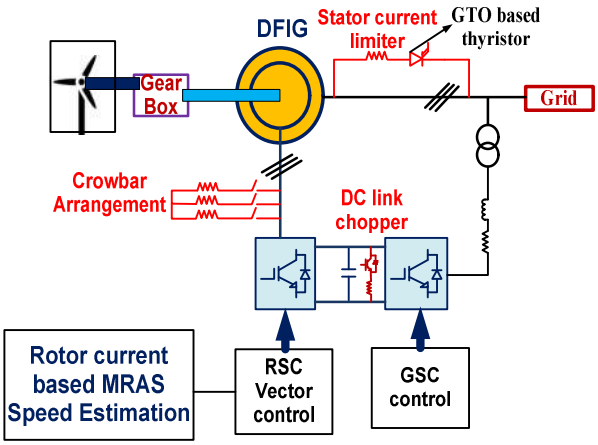

Fig. 1: Overall DFIG-wind turbine system with sensorless vector control and protection

978-1-4799-5141-3/14/$31.00 ©2016 IEEE

II. Modeling of DFIG

The stator and rotor voltage equations for DFIG in synchronously rotating *d-q* reference frame [5] are:

$$v_{ds} = R_s i_{ds} + \frac{d}{dt}\lambda_{ds} - \omega_e \lambda_{qs} \tag{1}$$

$$v_{qs} = R_s i_{qs} + \frac{d}{dt}\lambda_{qs} + \omega_e \lambda_{ds} \tag{2}$$

$$v_{dr} = R_r i_{dr} + \frac{d}{dt}\lambda_{dr} - (\omega_e - \omega_r)\lambda_{qr} \tag{3}$$

$$v_{qr} = R_s i_{qr} + \frac{d}{dt}\lambda_{qr} + (\omega_e - \omega_r)\lambda_{dr} \tag{4}$$

The flux linkage equations for both stator and rotor side equivalent circuit are:

$$\lambda_{ds} = L_s i_{ds} + L_m i_{dr} \tag{5}$$

$$\lambda_{dr} = L_s i_{dr} + L_m i_{ds} \tag{6}$$

$$\lambda_{qs} = L_s i_{qs} + L_m i_{qr} \tag{7}$$

$$\lambda_{qr} = L_r i_{qr} + L_m i_{qs} \tag{8}$$

The state space model of DFIG with stator and rotor currents as state variables is given by (9).

$$\begin{bmatrix} \frac{d}{dt} i_{ds} \\ \frac{d}{dt} i_{qs} \\ \frac{d}{dt} i_{dr} \\ \frac{d}{dt} i_{qr} \end{bmatrix} = \begin{bmatrix} -\frac{R_s}{L_s} & \omega_e & \frac{-sL_m}{L_s} & \frac{\omega_e L_m}{L_s} \\ \omega_e & -\frac{R_s}{L_s} & -\frac{\omega_e L_m}{L_s} & \frac{-sL_m}{L_s} \\ \frac{-sL_m}{L_s} & \frac{(\omega_e - \omega_r)L_m}{L_r} & -\frac{R_r}{L_r} & (\omega_e - \omega_r) \\ \frac{-(\omega_e - \omega_r)L_m}{L_r} & \frac{-sL_m}{L_s} & (\omega_e - \omega_r) & -\frac{R_r}{L_r} \end{bmatrix} \begin{bmatrix} i_{ds} \\ i_{qs} \\ i_{dr} \\ i_{qr} \end{bmatrix} + \begin{bmatrix} \frac{1}{L_s} & 0 & 0 & 0 \\ 0 & \frac{1}{L_s} & 0 & 0 \\ 0 & 0 & \frac{1}{L_r} & 0 \\ 0 & 0 & 0 & \frac{1}{L_r} \end{bmatrix} \begin{bmatrix} v_{ds} \\ v_{qs} \\ v_{dr} \\ v_{qr} \end{bmatrix} \tag{9}$$

Here, v is the voltage, i is the current, R is the resistance and ω_e and ω_r are the stator and rotor electrical angular velocity (rad/s), respectively, L_m is the mutual inductance between stator and rotor windings and λ is the flux linkage. Subscript s and r represent stator and rotor quantities respectively.

III. Sensorless Vector Control of DFIG

The stator flux oriented vector control with rotor current based MRAS controls the machine side converter of the DFIG. In this control scheme, the stator flux (q-axis) is maintained at zero while the resultant stator flux is same as d-axis stator flux as given in (10) [4]. Fig. 2 illustrates a block diagram of sensorless vector control of DFIG. The rotor voltages in the d-q reference frame for employing vector control is given by (11) and (12).

$$\lambda_s = \lambda_{ds} = L_m i_{ms} = L_s i_{ds} + L_m i_{dr} \qquad \lambda_{qs} = 0 \tag{10}$$

$$v_{dr} = R_r i_{dr} + \sigma L_r \frac{di_{dr}}{dt} - \omega_{slip} \sigma L_r i_{qr} \tag{11}$$

$$v_{qr} = R_r i_{qr} + \sigma L_r \frac{di_{qr}}{dt} + \omega_{slip}(L_m i_{ms} + \sigma L_r i_{dr}) \tag{12}$$

$$Leakage\ factor,\ \sigma = 1 - \frac{L_m^2}{L_s L_r} \tag{13}$$

The rotor current in the d-q frame is controlled using conventional PI controllers. The references for inner current control such as i_{dr} and i_{qr} are derived from outer reactive power control and speed control loop respectively. Here, the reactive power reference is set at zero to maintain unity power factor operation.

The rotor speed is estimated by using rotor current-based MRAS technique as proposed in [4]. The reference rotor current measured from transducers and rotor current of the adjustable model is estimated as given in (14).

$$\hat{i}_r = \frac{\lambda_s - L_s i_s}{L_m} e^{-j\hat{\theta}_r} \tag{14}$$

The MRAS observer error (E) is the cross product result of measured and estimated rotor current given by (15), which is fed to the PI controller and tuned to zero at estimated rotor speed.

$$E = i_r \otimes \hat{i}_r \tag{15}$$

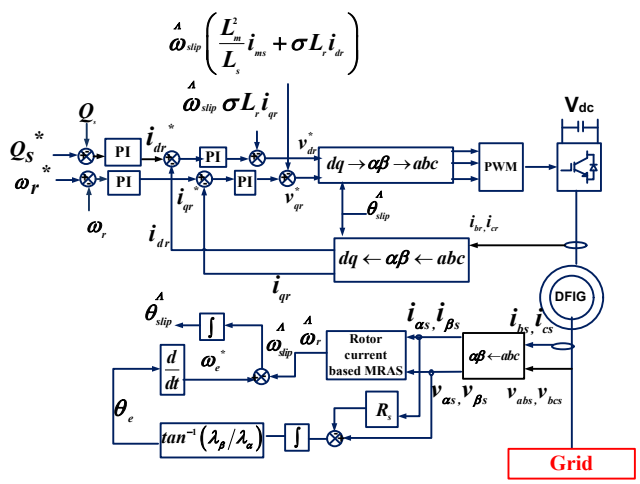

Fig. 2: Sensorless stator flux oriented vector control

IV. Supply Side Converter Control

The purpose of a supply side converter is to maintain dc bus voltage constant, control of grid side current with decoupled active and reactive power control. Phase locked loop (PLL) is used to derive the angle for *d-q* reference frame transformation such that the grid voltage vector aligns itself on the d-axis of the synchronously rotating reference frame. Fig. 3 represents the block diagram for grid side converter control. The modulating signals in the *d-q* reference frame for sine PWM gate pulse generation are given by (16) and (17) respectively. Control signal for reference voltage generation for inverter current control is given by (18) [7].

$$m_d = \frac{2}{V_{dc}}\left(u_d + \omega_s L i_q + v_d\right) \tag{16}$$

$$m_q = \frac{2}{V_{dc}}\left(u_q - \omega_s L i_d + v_q\right) \tag{17}$$

$$u = (k_p + \frac{k_i}{s})(i^* - i) \tag{18}$$

In the above equations, subscript d and q are quantities in *d-q* reference frame, V_{dc} is the dc bus voltage, ω_s is the grid angular frequency, v and i are grid voltage and current respectively, L is the line inductance between grid and grid side converter, k_p and k_i are proportional and integral gains for the current controllers.

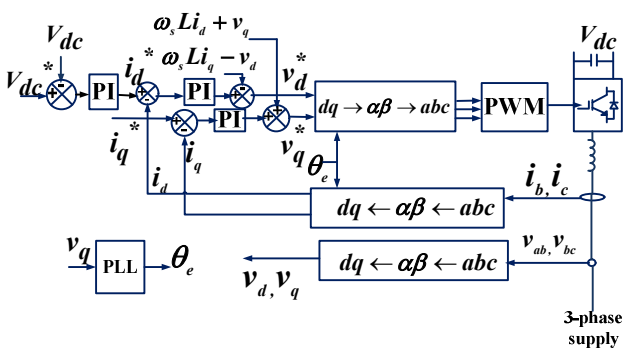

Fig. 3. Grid side converter control

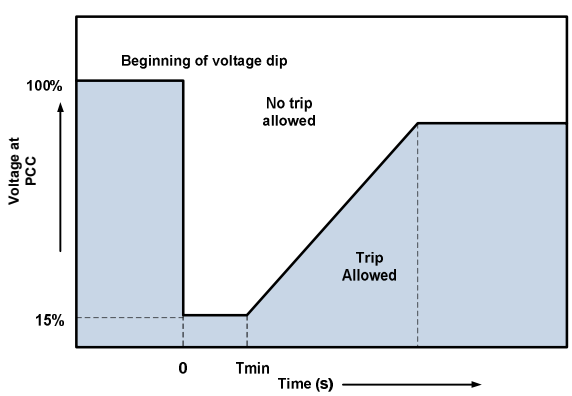

Fig. 4: Typical LVRT curve [8]

V. Low Voltage Ride-Through of DFIG

New grid codes require that the DFIG-based wind turbines remain connected while a voltage dip at the PCC occurs depending on the LVRT characteristics. This is necessary as sudden disconnection of DFIG can have a negative impact on the power system stability and safety. Fig. 4 illustrates a typical LVRT curve [8], which shows the grey zone as a trip zone where the DFIG must be disconnected to avoid hazardous situation while the white portion depicts a non-trip region where it can withstand the voltage dip. The steps involved in operating the crowbar system, stator current limiter and dc chopper is explained with the help of a flowchart as shown in Fig. 5. Here, a crowbar system which is an IGBT-based resistive network arrangement is programmed to operate when a voltage dip is detected. It is disabled with the restoration of steady state operating conditions. In this way, it protects the rotor side converter from large rotor current transients during the voltage sag. To prevent dc bus overvoltage, a dc chopper is connected to the dc bus and activates only after the voltage dip is detected. Stator current limiter is connected at stator side to limit the stator current to its threshold value.

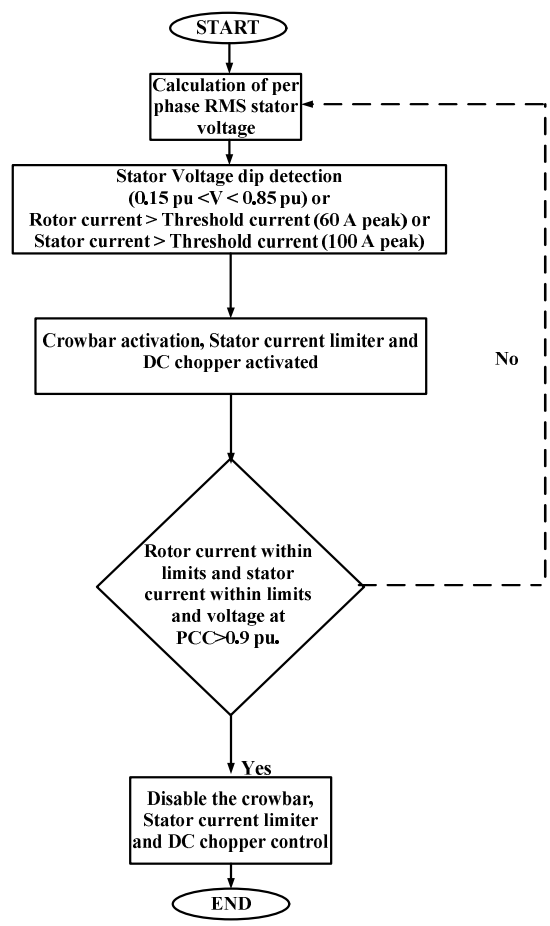

Fig. 5: Flowchart for protection during voltage dip.

With the detection of voltage sag at the point of common coupling of the DFIG, the gate signals are generated to turn on the IGBT operated crowbar system. Similarly, gate pulse is provided to IGBT for operating during the voltage sag up to restoration of normal operating conditions. After fault clearance, the rotor side converter current limits are checked before enabling its control action for a safe operation of the converter. The crowbar, stator current limiter, and dc chopper are disabled after the restoration period.

VI. Results

A DFIG set-up with back-to-back converter arrangement which is controlled based on sensorless vector control with LVRT capability is simulated in MATLAB/SIMULINK environment. The simulation parameters for the machine, converters and controllers (proportional constant, k_p and integral constant, k_i) used are mentioned in Appendix I.

A. Variable speed operation

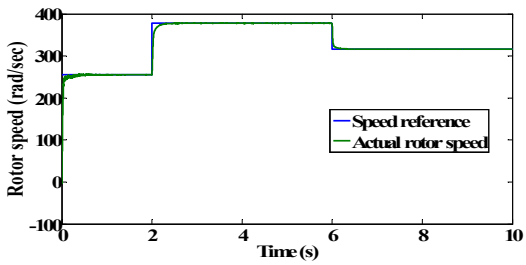

Fig. 6: Rotor speed

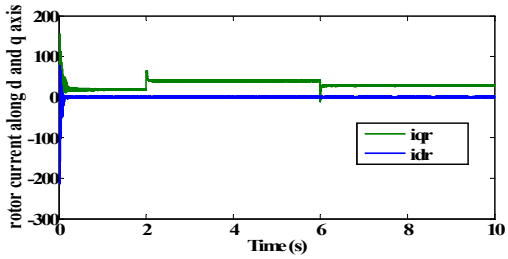

Fig. 7: Rotor current in d-q reference frame

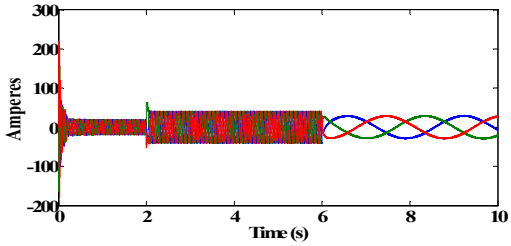

Fig. 8: Rotor current

B. Voltage dip condition and validation of sensorless vector control with LVRT operation.

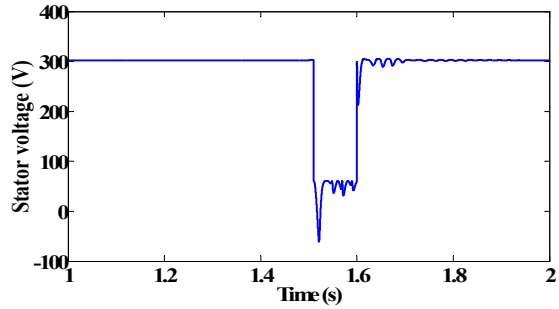

Fig. 9: Stator voltage with voltage dip

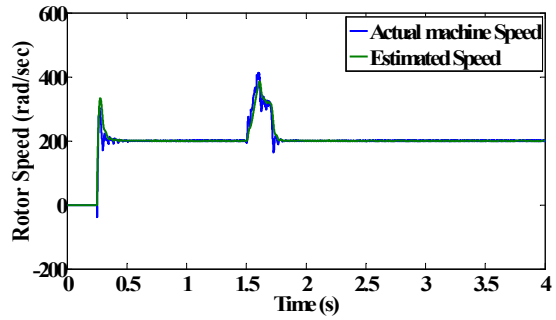

Fig. 10: Comparison of actual and estimated speedduring voltage dip

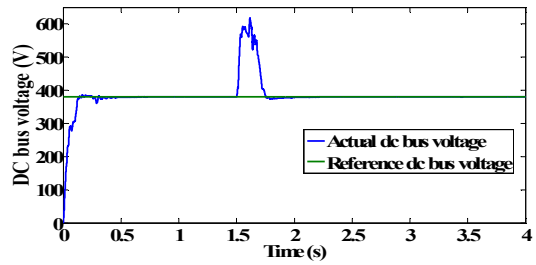

Fig. 11: DC bus voltage without dc chopper control during voltage dip

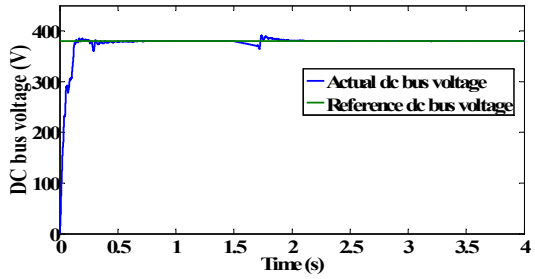

Fig. 12: DC bus voltage with dc chopper control during voltage dip

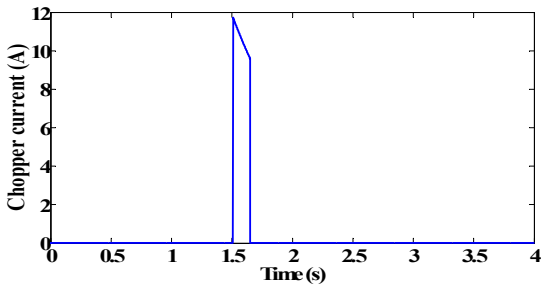

Fig. 13: DC chopper current

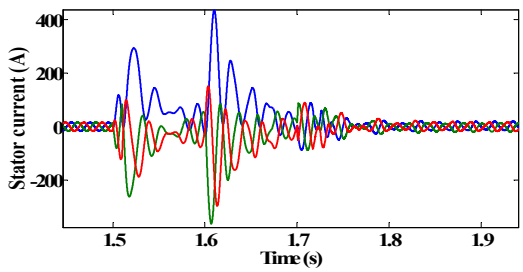

Fig. 14: Stator current without stator current limiter

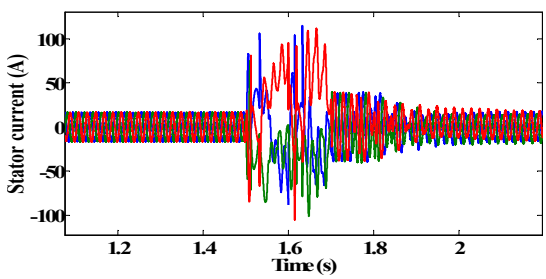

Fig. 15: Stator current with stator current limiter

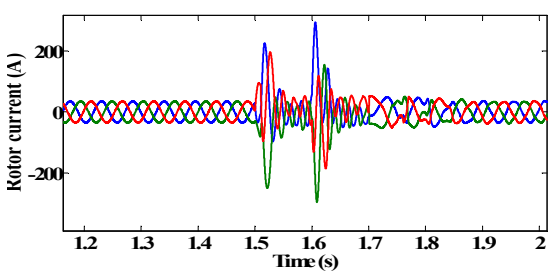

Fig. 16: Rotor current without crowbar protection

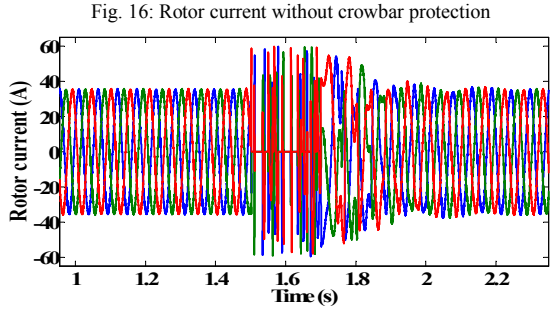

Fig. 17: Rotor current with crowbar protection

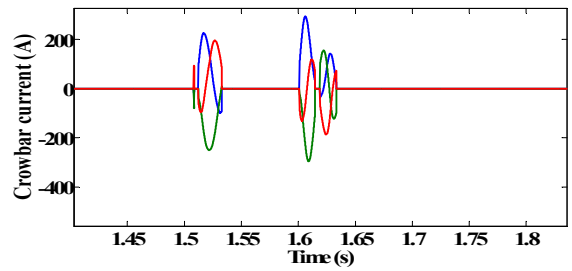

Fig. 18: Crowbar current

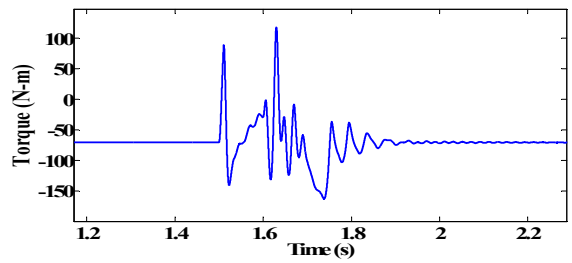

Fig. 19: Electromagnetic Torque without protection enabled

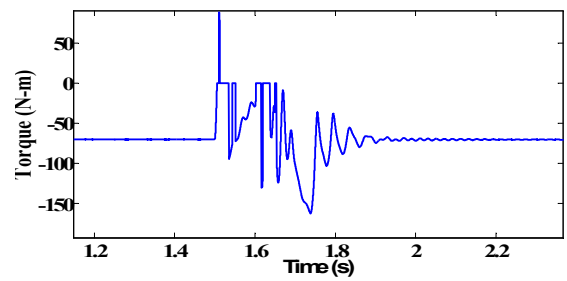

Fig. 20: Electromagnetic Torque with protection enabled

VII. Discussion

A. *Variable speed operation*

Since, DFIGs are mostly used in variable speed applications; initial steady state simulation for variable speed operation is carried out. The speed reference (ω_r^*) for the speed controller is set such that optimal energy is captured as given by [2].

$$\omega_r^* = \sqrt{\frac{T_m}{k_{opt}}} \tag{19}$$

$$k_{opt} = \frac{0.5 C_p \pi \rho r^5}{\lambda_o^3} \tag{20}$$

Here, T_m is the mechanical torque, C_p is the optimum turbine power coefficient, r is the turbine radius, ρ is the air density and λ_o is optimum tip speed ratio. For this part of simulation, reactive power controller is not required as reference for d-axis rotor current is set as zero. Fig. 6 illustrates the variation of rotor speed with set speed reference. The q-axis rotor current (i_{qr}) follows the variation in speed pattern and d-axis rotor current (i_{dr}) is maintained at zero as shown in Fig. 7. Similarly three phase rotor current with variable slip frequency can be observed in Fig. 8. It is observed in Fig. 8 that current after 6 s has low slip frequency as speed is 316.6 rad/sec which corresponds to 0.83% slip.

B. *Voltage dip condition and validation of sensorless vector control with LVRT operation.*

A voltage dip with 0.2 pu voltage seen at stator terminal is created starting at 1.51 s lasting up to 100 ms as shown in Fig. 9. The rotor current-based MRAS observer is used to estimate rotor speed here. The protection methodology is initiated after the voltage dip detection, satisfying the grid code for operating LVRT as shown in Fig. 5. From the observation of waveforms, it is evident that steady state operating conditions are restored at 1.95 s. The stator currents settle down to their nominal values at 1.95 s. With voltage dip, there is demagnetization of generator leading to increase in rotor speed as observed in Fig. 10. It is further verified that the actual speed computed from the inertia model of DFIG and estimated speed computed from rotor current-based MRAS are equal. Hence, the estimated speed is used for the vector control of the DFIG. The dc link chopper control has reduced the dc bus overvoltage from 617 V (1.62 pu) to nearly 390 V (1.02 pu) at the peak during the voltage sag condition as observed in Fig. 11 and Fig. 12 respectively. The chopper current in Fig. 13 is seen as a sharp rise of dc current during the activation period followed by steady dip after deactivation of chopper control. Stator current rises as high as 400 A in the absence of stator current limiter as shown in Fig. 14. With GTO-based thyristor controlled stator current limiter, the stator current is controlled up to 100 A peak or 70 A rms as seen in Fig. 15. Without and with crowbar activation, the rotor current is observed in Fig. 16 and Fig. 17 respectively. The crowbar current during the voltage dip is shown in Fig. 18. Fig. 19 and Fig. 20 illustrate the electromagnetic torque variation with and without the protection enabled respectively. The torque pulsates even after fault removal and reaches its steady state value of -71 N-m at 2.2 seconds.

VIII. CONCLUSION

This paper presents a sensorless vector control using rotor current-based MRAS technique with LVRT of DFIG. With speed estimation being employed, the issues with speed encoder are no longer applicable. Further, the protection strategy is to ensure a safe and stable operation of the system. As the system parameters computed are from an experimental DFIG setup, this simulation will be useful for proceeding towards the experimental validation.

APPENDIX I

Table I: Controller Parameters

Controlled variable	k_p	k_i
Speed estimation	1	100
Speed control	0.8	11
Reactive power	0	10
d-axis rotor current, i_{dr}	5	50
q-axis rotor current, i_{qr}	5	50
d-axis grid current, i_d	1	10
q-axis grid current, i_q	1	10

Table II: DFIG and grid side parameters

Parameter	Values
Rated power of DFIG	22 kW
Rated Stator voltage	415 VL-L
Rated Stator current	44 A
Rated Rotor current	29 A
DC bus voltage	380 V
Stator resistance	0.083 ohm
Stator leakage inductance	1.665 mH
Rotor resistance (referred to stator side)	0.167 Ω
Rotor leakage inductance (referred to stator side)	1.665 mH
Magnetizing inductance	0.032 H
Rotor Inertia (J)	0.1 kg/m^2
Pole pairs	3
Grid side Transformer	180V /415 V L-L
Grid side resistance (R)	0.1Ω
Grid side Inductance (L)	2 mH
Grid side converter power rating	15 kVA
Rotor side converter power rating	10 kVA

Acknowledgment

The authors are thankful to Indian Institute of Technology Kharagpur for its support and permission to present this paper.

References

[1] A. Petersson, “Analysis, modeling and control of doubly-fed induction generators for wind turbines”, Chalmers Univ., Göteborg, Sweden, 2003.

[2] R. Pena, J. C. Clare, and G. M. Asher, “Doubly fed induction generator using back-to-back PWM converters and its application to variablespeed wind-energy generation,” *Proc. Inst. Elect. Eng., Electr. Power Appl.*, vol. 143, no. 3, pp. 231–241, May 1996.

[3] R. Cardenas, R. Pena, J. Clare, G. Asher, and J. Proboste, “MRAS observers for sensorless control of doubly-fed induction generators,” *IEEE Trans. Power Electron.*, vol. 23, no. 3, pp. 1075–1084, May 2008.

[4] R. Pena, R. Cardenas, J. Proboste, G. Asher, and J. Clare, “Sensorless control of a slip ring induction generator based on rotor current MRAS observer,” in *Proc. 36th IEEE PESC*, 2005, pp. 2508–2513.

[5] B. K. Bose,“Power electronics and motor drives: advances and trends”, Academic press, 2010.

[6] Johan Morren and Sjoerd WH De Haan. "Ridethrough of wind turbines with doubly-fed induction generator during a voltage dip." *IEEE Trans. Energy conversion, vol.* 20, no .2, pp. 435-441, 2005.

[7] A. Yazdani, and I. Reza, “Voltage-sourced converters in power systems: modeling, control, and applications”, *John Wiley & Sons*, 2010.

[8] M. Ezzat, *et al*. "Low-voltage ride-through techniques for DFIG-based wind turbines: State-of-the-art review and future trends." *Industrial Electronics Society, IECON 2013-39th Annual Conference of the IEEE*, IEEE, 2013.

[9] N. H. Saad, Ahmed A. Sattar, and Abd El-Aziz M. Mansour. "Low voltage ride-through of doubly-fed induction generator connected to the grid using sliding mode control strategy." *Renewable Energy*, vol. 80, pp.583-594, 2015.